Spectral states evolution of 4U 1728-34 observed by INTEGRAL and RXTE: non-thermal component detection

Tarana, A.; Belloni, T.; Bazzano, A.; Mendez, M.; Ubertini, P.

Published in:
Monthly Notices of the Royal Astronomical Society

DOI:
10.1111/j.1365-2966.2011.18951.x

Publication date:
2011

Monthly Notices
of the
ROYAL ASTRONOMICAL SOCIETY

Mon. Not. R. Astron. Soc. **416,** 873–880 (2011) doi:10.1111/j.1365-2966.2011.18951.x

Spectral states evolution of 4U 1728–34 observed by *INTEGRAL* and *RXTE*: non-thermal component detection

A. Tarana,[1]⋆ T. Belloni,[2] A. Bazzano,[1] M. Méndez[3] and P. Ubertini[1]

[1]*Istituto di Astrofisica Spaziale e Fisica Cosmica – INAF, via del Fosso del Cavaliere 100, I-00133 Roma, Italy*
[2]*Osservatorio Astronomico di Brera – INAF, Via E. Bianchi 46, I-23807 Merate (LC), Italy*
[3]*Kapteyn Astronomical Institute, University of Groningen, PO Box 800, 9700 AV Groningen, the Netherlands*

Accepted 2011 April 20. Received 2011 April 20; in original form 2010 December 7

ABSTRACT

We report results of a one-year monitoring of the low-mass X-ray binary (LMXB) source (atoll type) 4U 1728–34 with *INTEGRAL* and *RXTE*. Three time intervals were covered by *INTEGRAL*, during which the source showed strong spectral evolution. We studied the broad-band X-ray spectra in detail by fitting several models in the different sections of the hardness–intensity diagram. The soft states are characterized by prominent blackbody emission plus a contribution from a Comptonized emission. The hard states are characterized by the presence of an excess flux with respect to the Comptonization model above 50 keV, while the soft component is fainter. To obtain an acceptable fit to the data, this excess is modelled either with a power law with photon index $\Gamma \sim 2$ or a Comptonization (CompPS) spectrum implying the presence of hybrid thermal and non-thermal electrons in a corona. This makes 4U 1728–34 one of the few LMXBs of atoll type showing non-thermal emission at high energy. From our analysis, it is also apparent that the presence of the hard tail is more prominent as the overall spectrum becomes harder. We also discuss alternative models which can describe these hard states.

Key words: stars: neutron – X-rays: binaries – X-rays: individual: 4U 1728-34.

1 INTRODUCTION

X-ray binaries show different spectral states depending on the different contributions of the emission components. The neutron star low-mass X-ray binary (NS LMXB) spectra are complex and difficult to explain, and the precise origin of the spectral components is still debated. Different models in fact can describe the same observed spectra. Historically, concerning the soft X-ray range (1–20 keV), two main models were used for the X-ray spectra of LMXBs: (i) the 'eastern model' consists of the sum of an optically thick multitemperature disc, plus a Comptonized blackbody originating from the neutron star or boundary layers between the disc and the neutron star (Mitsuda et al. 1984, 1989) and (ii) the 'western model' uses a Comptonized spectrum due to repeated inverse Compton scattering of the soft seed photons by hot electrons with a thermal distribution of velocities, plus a single-temperature blackbody emission (White et al. 1986).

In the past years, observations in the hard X-ray bands (>20 keV) also indicated that broad-band spectral studies are necessary to model and explain all the components and features observed in the soft and hard spectral states of NS LMXBs.

During the soft spectral state, the soft thermal component is predominant. The thermal component could come from different emission regions or combination of these, such as either the optically thick and geometrically thin accretion disc that emits as a blackbody with a local temperature depending on the disc radius [$T(R) \propto R^{-3/4}$], or the thermal surface of the NS, or the NS boundary layers. Indeed, the emission regions of these components are generally known although difficult to discern from the observed spectra.

During the hard spectral state the soft component decreases or is even not detected, while the contribution of the Comptonization component due to the repeated Compton upscattering of the soft photons in a hot electron cloud (corona) is predominant in the spectra.

The hard component could extend above 200 keV, and in some cases no cut-off at high energy is observed (Piraino et al. 1999; Di Salvo et al. 2000a, 2001a; Iaria et al. 2001), which is the signature for non-thermal emission. The spectral state transition from soft to hard states is often modelled in terms of a gradual increase of the electron temperature of the Comptonizing region which is typically in the range of 3–10 keV for the soft states and it increases to the range 10–100 keV for the hard ones.

Moreover, depending on the geometry of the binary system and on the position of the disc with respect to the observer, the additional reflection component could be present in the spectra of the LMXBs.

⋆E-mail: antonella.tarana@iasf-roma.inaf.it

This is due to Compton reflection of the hard X-ray by material of the accretion disc (Di Salvo & Stella 2002).

Recently, Lin, Remmilard & Homan (2007) applied a new model for the high-luminosity soft states of LMXBs with NS, inspired to the black hole binaries (BHBs) behaviour. This model consists of blackbody plus multicolour disc blackbody with no need for a strong Comptonized emission. However, as the luminosity decreases, the Comptonized component is required also for this model.

4U 1728–34 is an LMXB of the atoll class (Forman, Tananbaum & Jones 1976; Hasinger & van der Klis 1989; Di Salvo et al. 2001b; van Straaten et al. 2002) containing an NS as indicated by the observation of type I X-ray bursts (Hoffman et al. 1976; Lewin, Clark & Doty 1976). The detection of Eddington-limited bursts allowed a distance estimate of 4.4–5.1 kpc (Di Salvo et al. 2000b; Galloway et al. 2003).

The X-ray spectrum of the persistent emission of 4U 1728–34 over a wide energy band has been studied with different satellites in the past years: *Einstein* (Grindlay & Hertz 1981), *GRANAT* (Claret et al. 1994), *BeppoSAX* (Di Salvo et al. 2000b; Piraino 2000), *Chandra*, *RXTE* (D'Aí et al. 2005) and *INTEGRAL* (Falanga et al. 2006). The broad-band spectra were modelled with a disc blackbody emission plus a thermal-Comptonization component with varying optical depth and electron temperature (Di Salvo et al. 2000b; Farinelli et al. 2004; Falanga et al. 2006). Residuals from the fit in the 6–9 keV interval were interpreted either as a broad ($\sigma \sim 0.3$–0.7) Gaussian emission line at 6.7 keV or as two absorption edges of ionized iron at 7 and 9 keV (Piraino 2000; D'Aí et al. 2006).

4U 1728–34 is one of the few atoll sources detected in the radio band up to now (Martí et al. 1998; Migliari et al. 2003). The radio and X-ray fluxes follow a correlation similar to that found for BHBs and Z sources which are typically more luminous than atolls (Fender 2006; Migliari & Fender 2006). Z and BH sources could show a non-thermal tail in the X-ray energy spectra; the presence of this hard tail seems to be correlated with the position of the source in the colour diagram and the radio properties (Migliari et al. 2007). The analysis of non-thermal spectral components in atoll sources is, in general, more complex than in brighter X-ray binaries due to the low statistics involved, though *INTEGRAL* recently provided important results (Fiocchi et al. 2006; Tarana et al. 2007). The hard tail component could originate from a hybrid thermal/non-thermal population of electrons in a corona near the compact object (e.g. Poutanen & Coppi 1998) as already revealed in the atoll 4U 1820–30 in its hard state (Tarana et al. 2007). Alternatively, the hard tail component could originate from non-thermal electrons coming from the base of a jet (Markoff, Nowak & Wilms 2005). The bulk motion Comptonization model (Titarchuk & Zannias 1998), applied usually for BH, was recently also used in NS (CompTB model) and represents an alternative physical explanation of the detected hard tails (Farinelli, Titarchuk & Frontera 2007; Farinelli et al. 2008).

In this work, we analyse data from a year-long *RXTE*/*INTEGRAL* monitoring campaign of 4U 1728–34 and show a non-thermal tail detected in the X-ray spectra of this source.

2 THE OBSERVATION CAMPAIGN

The *INTEGRAL* monitoring of 4U 1728–34 consists of two parts: the first (2006 February–April) is part of Galactic Centre Deep Exposure observations and the second of Key Programme pointings as well as public data (General Programme) (2006 August–October and 2007 February–April). The total pointings with our target positioned in the fully coded field of view (FCFOV) are 496 (about 2000 s each). We extracted light curves in the 20–40, 40–100 and 100–300 keV energy bands with IBIS.

INTEGRAL data were processed using the Off-line Scientific Analysis (OSA version 7.0; Goldwurm et al. 2003) software released by the ISDC (Courvoisier et al. 2003).

For spectral extraction, all the available data for which the source was within the IBIS/ISGRI FCFOV ($4.5^\circ \times 4.5^\circ$) were analysed, so that the flux evaluation is not affected by calibration uncertainties in the off-axis response.

A 2 per cent systematic error to IBIS/ISGRI data sets was added,[1] and the standard 2048 channels response matrix logarithmically rebinned to 62 channels was used.

The *RXTE* monitoring consists of 2 ks pointings every 2 d, from 2006 March to 2007 June. We extracted the 3–20 keV light curve from PCA and energy spectra from the PCA and HEXTE instruments (background- and dead-time-corrected) for each observation using the *RXTE* software within HEASOFT v. 6.6.3, following the standard procedures. For spectral analysis, only proportional counter unit 2 (PCU2) from the PCA and Cluster B from HEXTE were used. A systematic error of 0.6 per cent was added to the PCA spectra to account for uncertainties in the instrument calibration. We accumulated background-corrected PCU2 rates in the channels A = 7–48 (2.87–20.20 keV), B = 7–13 (2.87–5.71 keV) and C = 14–23 (5.71–9.81 keV). The hardness–intensity diagram (HID) was constructed as H = C/B versus the total rate A (see Homan & Belloni 2005). One rate/hardness point was extracted for each observation.

2.1 Light curves

Fig. 1 (top three panels) shows the IBIS and PCA light curves of the total observing period in the 20–40 and 3–20 keV energy bands; the bottom panel shows the time evolution of the PCA hardness ratio corresponding to the count rate ratio 5.71–9.81/2.87–5.71 keV. In the three intervals with simultaneous *INTEGRAL*–*RXTE* coverage, both flux and hardness show evident changes. A zoom-in of the second period is shown in the bottom three panels of Fig. 1.

Fig. 2 shows the IBIS light curves for the FCFOV pointings in the 20–40, 40–100 keV and in the top panel the 2–12 keV rate of the *RXTE*/ASM.[2] Note that during each *INTEGRAL* observation period a slow monotonic flux increasing in rate followed by a sharp drop is detected.

The anticorrelation of the soft and hard flux indicates a spectral change of the source, as confirmed by its track through the PCA HID of Fig. 3.

2.2 The hardness–intensity diagram

Fig. 3 shows the HID for PCA/*RXTE* data. Different colours correspond to the three periods for which we have simultaneous data from *RXTE* and *INTEGRAL*: red, blue and green points for the first, second and third period, respectively. The empty points correspond to PCA data without *INTEGRAL* coverage. In each period, the source moves steadily from the soft to the hard states and back to the soft state following a counterclockwise path. From the HID, we selected six boxes (shown in Fig. 3) and derived energy spectra (hereafter spe1 through spe6) by adding data within each box. In this way, we combine *INTEGRAL* and *RXTE* data corresponding to each different spectral state.

[1] http://isdc.unige.ch/?Support+documents
[2] http://xte.mit.edu/ASM_lc.html

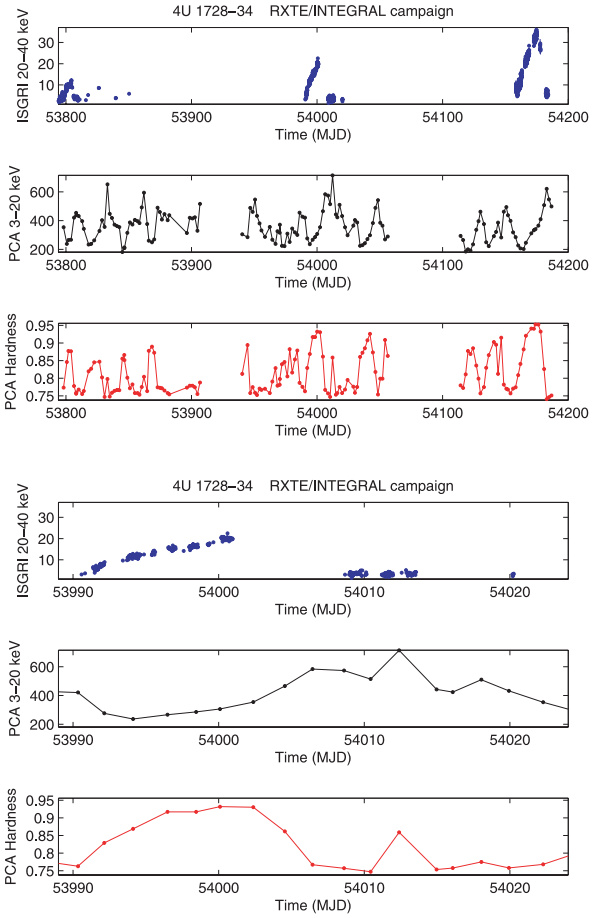

Figure 1. Top: *INTEGRAL*/IBIS and *RXTE*/PCA 2006–2007 light curves of 4U 1728–34. Three main periods of observation are visible. PCA hardness (5.71–9.81 keV/2.87–5.71 keV count rate ratio) is shown in the third panel. Bottom: zoomed-in light curve during the second period.

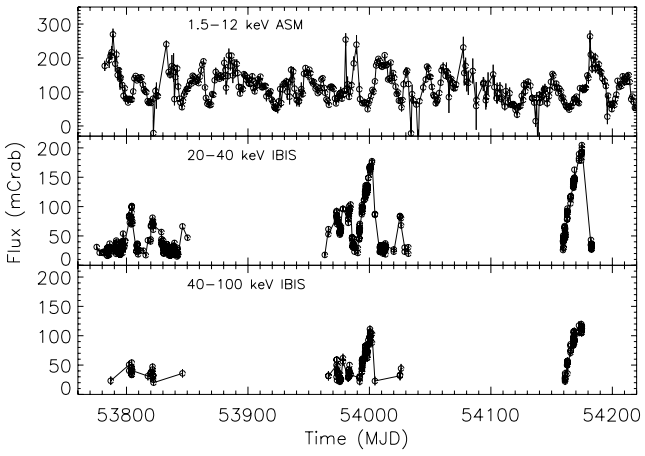

Figure 2. *INTEGRAL*/IBIS and *RXTE*/ASM 2006–2007 light curves of 4U 1728–34. The energy bands are indicated for each panel.

The spectral grouping based on the time evolution of the data, keeping the three observation periods separately, gives spectral changes consistent with the results obtained using the spectra from the selected boxes. We use spectra from the HID boxes which have large signal-to-noise ratio by adding data of the three periods and by covering a rather large range in count rates. We nevertheless

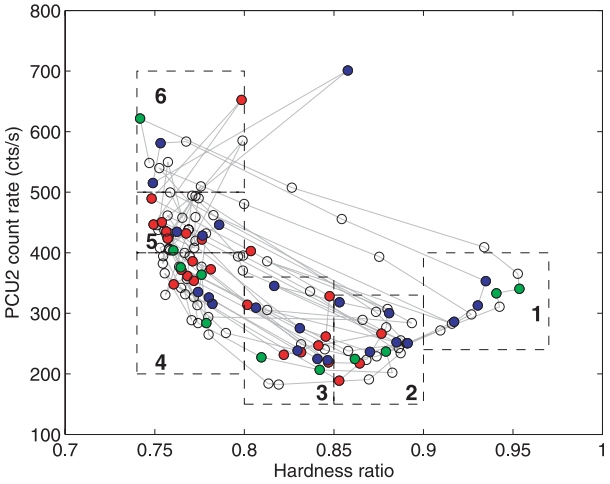

Figure 3. Hardness–intensity diagram of 4U 1728–34 with PCA data. The hardness is the count rate ratio of the bands (5.71–9.81 keV)/(2.87–5.71 keV) and the intensity is the count rate in the 2.87–20.20 keV. Different colours are used for the three different observing periods (see text). The source covers the atoll track moving from the soft (box 6) to the hard (box 1) states, then jumping back to soft.

checked that the spectra of single observation within each box did not deviate significantly from each other and also that there are no systematic differences between the three periods.

Boxes 1–3 correspond to intervals when the source spectrum was hard (corresponding to the flux maxima of the *INTEGRAL* light curves), while boxes 4–6 correspond to intervals when the source spectrum was soft.

Note that during the first period 4U 1728–34 did not reach values of hardness as high as in the other periods (no red points are in box 1).

2.3 Spectral analysis

We analysed the spe1–spe6 spectral data sets (see Fig. 3) of the *INTEGRAL*/IBIS and *RXTE*/PCA and HEXTE simultaneous observations using XSPEC version 12.5.1 (Arnauld et al. 1996).

During the fitting, a multiplicative constant, frozen to 1 for PCA and a value ranging from 0.7 to 0.9 for IBIS/ISGRI and HEXTE, is added, to account for uncertainties in the cross-calibration of the three instruments.

For the spectral fits, we used data in the 3.5–25 keV band for PCA and above 20 and 19 keV for HEXTE and IBIS, respectively.

For the different spectral states, we attempted several combinations of models. To fit a broad emission line, we added a Gaussian component that was fixed at the best-fitting value comprised in $\sigma_{\rm Fe} \sim 0.3$–0.7 and at about 6.5 keV, compatible with previously observed values (Piraino 2000; D'Aí et al. 2005). We fixed the interstellar column density to $N_{\rm H} = 2.3 \times 10^{22}$ cm^{-2}, as deduced from previous observations below 3 keV (D'Aí et al. 2006).

We found it difficult to statistically constrain the soft parameters (the blackbody temperature and normalization, and also the seed photons temperatures of the Comptonization component) probably due to the lack of data coverage at low energy ($\lesssim$3.5 keV). Hence, in some cases we fixed the soft parameters to the best-fitting value.

(1) CompTT model

Only spectra spe5 and spe6 are well represented with a simple Comptonization model, assumed with a disc geometry, CompTT (Titarchuk 1994), as reported in Table 1. The results for spectra

Table 1. Spectral fitting results for the spectra of 4U 1728–34 with simultaneous *INTEGRAL* and *RXTE* observations.

	spe1	spe2	spe3	spe4	spe5	spe6
Parameters			CompTT (1)			
kT_0 (keV)	$0.85^{+0.02}_{-0.02}$	$0.87^{+0.02}_{-0.02}$	0.95 ± 0.01	$0.82^{+0.05}_{-0.04}$	0.50 ± 0.06	$0.72^{+0.05}_{-0.04}$
kT_e (keV)	$12.3^{+0.39}_{-0.37}$	$11.99^{+0.54}_{-0.69}$	7.33 ± 0.23	$3.18^{+0.05}_{-0.05}$	$3.10^{+0.05}_{-0.02}$	$3.02^{+0.03}_{-0.03}$
τ	$2.62^{+0.06}_{-0.06}$	$2.37^{+0.12}_{-0.07}$	2.81 ± 0.08	$5.44^{+0.14}_{-0.15}$	$5.75^{+0.05}_{-0.06}$	$5.73^{+0.09}_{-0.13}$
$\text{norm}_{\text{CompTT}} \times 10^{-2}$	$5.84^{+0.21}_{-0.21}$	$4.61^{+0.34}_{-0.26}$	7.65 ± 0.28	$29.65^{+1.56}_{-1.24}$	$53.55^{+3.89}_{-2.79}$	$59.81^{+2.75}_{-2.85}$
$\chi^2_r(\nu)$	1.51(98)	1.45(88)	2.32(73)	1.95(47)	1.17(58)	0.88(52)
			CompTT+bb (2)			
kT_0 (keV)	$0.93^{+0.07}_{-0.06}$	$0.89^{+0.04}_{-0.03}$	$0.76^{+0.04}_{-0.05}$	$0.70^{+0.04}_{-0.04}$	$0.69^{+0.05}_{-0.25}$	$0.79^{+0.04}_{-0.05}$
kT_e (keV)	$12.17^{+0.44}_{-0.41}$	$11.96^{+0.61}_{-0.57}$	$9.31^{+1.37}_{-0.95}$	$6.67^{+1.51}_{-1.25}$	$5.45^{+0.33}_{-0.77}$	$4.13^{+0.05}_{-0.13}$
τ	$2.64^{+0.08}_{-0.08}$	$2.37^{+0.09}_{-0.07}$	$2.41^{+0.25}_{-0.30}$	$2.26^{+0.52}_{-0.46}$	$2.63^{+0.15}_{-0.19}$	$3.28^{+0.18}_{-0.14}$
$\text{norm}_{\text{CompTT}} \times 10^{-2}$	$5.46^{+0.31}_{-0.32}$	$4.49^{+0.15}_{-0.28}$	$6.24^{+0.82}_{-0.89}$	$12.53^{+3.49}_{-2.77}$	$19.48^{+14.6}_{-3.45}$	$34.46^{+3.71}_{-2.84}$
kT_{bb} (keV)	$0.89^{+0.18}_{-0.23}$	$0.30^{+0.40}_{-0.29}$	$2.48^{+0.22}_{-0.19}$	$2.34^{+0.42}_{-0.43}$	$2.39^{+0.04}_{-0.04}$	2.44 ± 0.05
$\text{norm}_{\text{bb}} \times 10^{-3}$	$1.75^{+0.6}_{-0.4}$	$35.89^{+1.55}_{-2.83}$	$4.50^{+0.53}_{-0.55}$	$19.18^{+3.12}_{-0.87}$	$23.25^{+0.78}_{-0.61}$	$29.93^{+85.31}_{-0.64}$
$\chi^2_r(\nu)$	1.61(96)	1.39(82)	0.99(71)	0.82(56)	0.94(56)	0.91(50)
			CompTT+PL (3)			
kT_0 (keV)	$0.85^{+0.08}_{-0.04}$	$0.89^{+0.09}_{-0.04}$	$1.17^{+0.07}_{-0.06}$	–	–	–
kT_e (keV)	$10.05^{+0.59}_{-0.60}$	$9.14^{+0.80}_{-0.67}$	$5.75^{+0.36}_{-0.19}$	–	–	–
τ	$2.99^{+0.25}_{-0.15}$	$2.84^{+0.25}_{-0.19}$	$3.49^{+0.12}_{-0.15}$	–	–	–
$\text{norm}_{\text{CompTT}} \times 10^{-2}$	$5.93^{+0.8}_{-1.1}$	$4.84^{+1.04}_{-1.05}$	$5.19^{+0.59}_{-0.63}$	–	–	–
Γ	$1.83^{+0.22}_{-0.55}$	$1.92^{+0.09}_{-0.04}$	$2.48^{+0.09}_{-0.07}$	–	–	–
norm_{PL}	$0.15^{+0.28}_{-0.14}$	$0.17^{+0.30}_{-0.15}$	$0.99^{+0.21}_{-0.15}$	–	–	–
$\chi^2_r(\nu)$	0.88(96)	0.89(84)	0.60(71)	–	–	–
			bb+diskbb+bknpower+higheut (4a)			
Γ_1	$1.39^{+0.08}_{-0.10}$	$1.59^{+0.09}_{-0.08}$	$1.90^{+0.07}_{-0.06}$	2.08 ± 0.16	2.44 ± 0.07	2.50 ± 0.61
E_{break}	$14.15^{+0.60}_{-0.61}$	$13.96^{+1.05}_{-0.87}$	$14^{+0.77}_{-0.72}$	18(fx)[a]	18(fx)	18(fx)
Γ_2	$1.89^{+0.05}_{-0.05}$	$2.04^{+0.10}_{-0.09}$	$2.48^{+0.11}_{-0.11}$	3.34 ± 0.17	3.03 ± 0.22	3.81 ± 0.82
$\text{norm}_{\text{bknpower}}$	$0.29^{+0.07}_{-0.07}$	$0.35^{+0.08}_{-0.07}$	$0.64^{+0.11}_{-0.09}$	0.29 ± 0.22	0.69 ± 0.13	0.45 ± 0.30
$E_{\text{cut-off}}$	$22.13^{+1.74}_{-1.30}$	$21.12^{+0.80}_{-0.67}$	$19.44^{+1.41}_{-1.34}$	–	–	–
E_{fold}	$48.70^{+3.97}_{-3.70}$	$48.23^{+3.62}_{-1.74}$	$38.52^{+8.80}_{-5.76}$	–	–	–
kT_{bb} (keV)	$1.43^{+0.02}_{-0.02}$	$1.46^{+0.05}_{-0.04}$	$1.59^{+0.08}_{-0.06}$	2.42 ± 0.01	2.54 ± 0.01	2.71 ± 0.02
norm_{bb}	$24.9^{+5.32}_{-4.81}$	$16.72^{+4.65}_{-4.22}$	$11.47^{+3.37}_{-3.11}$	6(fx)	6(fx)	6(fx)
kT_{in} (keV)	–	–	–	1.47 ± 0.02	1.54 ± 0.01	1.78 ± 0.01
$\text{norm}_{\text{diskbb}}$	–	–	–	30(fx)	30(fx)	30(fx)
$\chi^2_r(\nu)$	0.62(92)	0.75(81)	0.49(70)	0.79(48)	0.75(59)	0.85(53)
			CompTT+bb+diskbb+PL (4b)			
kT_0 (keV)	0.89 ± 0.08	1.0(fx)	0.95 ± 0.12	1.0(fx)	1.0(fx)	–
kT_e (keV)	10.47 ± 0.53	8.76 ± 0.38	6.55 ± 1.57	5.46 ± 0.69	4.99 ± 0.56	–
τ	2.87 ± 0.10	2.97 ± 0.10	3.12 ± 0.71	3.21 ± 0.77	3.59 ± 0.60	–
$\text{norm}_{\text{CompTT}} \times 10^{-2}$	5.89 ± 0.37	4.44 ± 0.19	6.80 ± 1.29	6.77 ± 2.35	6.52 ± 1.23	–
kT_{bb} (keV)	0.68 ± 0.34	0.96 ± 0.06	2.09 ± 0.41	2.22 ± 0.06	2.34 ± 0.03	2.76 ± 0.01
norm_{bb}	21.44 (fx)	16(fx)	1.1(fx)	6.64 ± 0.55	7.5(fx)	5.96 ± 0.039
kT_{in} (keV)	–	–	0.49 ± 0.09	0.93 ± 0.04	1.13 ± 0.17	1.74 ± 0.04
$\text{norm}_{\text{diskbb}}$	–	–	1575(fx)	163(fx)	98(fx)	37.11 ± 1.68
Γ	1.72 ± 0.01	1.9 ± 0.07	2 ± 1.1	–	–	–
norm_{PL}	0.08 ± 0.06	0.16 ± 0.06	0.11 ± 0.57	–	–	–
$\chi^2_r(\nu)$	1.09(94)	0.84(84)	0.74(71)	0.88(47)	0.76(59)	0.87(54)
F_{bol} (erg s^{-1} cm^{-2})[b]	8.5×10^{-9}	6.6×10^{-9}	5.8×10^{-9}	7.1×10^{-9}	8.2×10^{-9}	1.1×10^{-8}

[a](fx) are fixed parameters.

[b]The fluxes are extracted by the CompPS plus diskbb models for the spe1–spe3 data and by model (4b) for the spe4–spe6 data.

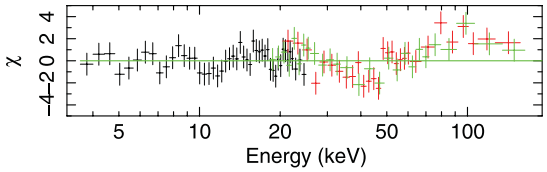

Figure 4. Residual to the CompTT models of the spe1 data set, without the power-law component.

spe1–spe3 are not acceptable due to an excess in the residuals at high energy (at $E > 50$ keV, from IBIS and HEXTE; see Fig. 4). We verified that this excess is not due to the procedure of combining spectra as it is also present in the individual spectra. Moreover, for spe3 and spe4 also a low-energy excess (below 5 keV) is detected, probably due to the presence of a soft blackbody emission.

The spectrum spe6 is shown in Fig. 5. The unabsorbed bolometric flux of the softest spectral state, spe6, is 1.1×10^{-8} erg cm^{-2} s^{-1} corresponding to a luminosity of 2.8×10^{37} erg s^{-1}, assuming a distance of 4.6 kpc (Di Salvo et al. 2000b; Galloway et al. 2003).

(2) CompTT+bb models

Adding a disc blackbody emission to the Comptonization component, diskbb (Mitsuda et al. 1984), the fits improve for the soft states [the χ^2_r(d.o.f.) is of 1.34(45), 0.85(56) and 0.87(50), respectively, for spe4, spe5 and spe6] though this component is not statistically significant because the normalization is not constrained. The fits with the addition of a single blackbody (bb) are better constrained and the results are reported in Table 1. Note that the χ^2_r is acceptable for all the soft states and also for spe3 even if the residuals to the models still reveal an excess above 50 keV. For spe1 the χ^2_r is worse than that of a simple Comptonization component, and for spe2 the best-fitting temperature of the blackbody is very low and difficult to constrain. In conclusion, the CompTT+bb model can be applied to the soft states for which the blackbody temperature decreases and the electron plasma temperature increases from spe6 to spe4. For the hard states, the spectral parameters (τ and $kT_{\rm bb}$) do not change monotonically from spe3 to spe1 (as the source becomes harder) as in general observed for these type of sources; moreover, the χ^2_r is not good (see spe1 results). So for hard states it is statistically difficult to constrain the possible soft component together with the Comptonization model.

(3) CompTT+PL models

To take into account the high-energy residuals observed with the simple Comptonization model during the hard state, we add a power-law component. This component is not required for the soft states. The best-fitting parameters of all hard state observations are shown in Table 2. The power-law component becomes less steep as the high-energy flux (at >50 keV) contribution increases.

This is visible in the energy spectra and residuals to the models of spe1 and spe3 which are shown in Fig. 5.

(4) bb+diskbb

For spe6, corresponding to the highest luminous state, a simple double blackbody emission (i.e. bb plus diskbb) gives good fit to the data (χ^2_r of 0.9), while for the other soft states and for the hard states the fits are not acceptable (the χ^2_r gives values of 1.8 and 2.5 for spe5 and spe4 and become worse for hard states). The blackbody emission obtained for spe6 is higher (2.7 keV) than the value obtained with model (2), and the inner disc temperature is 1.74 keV.

The high-energy emission contribution increases as the source goes to hard states, so other components than the double blackbody are necessary. We try to use two different hard components as

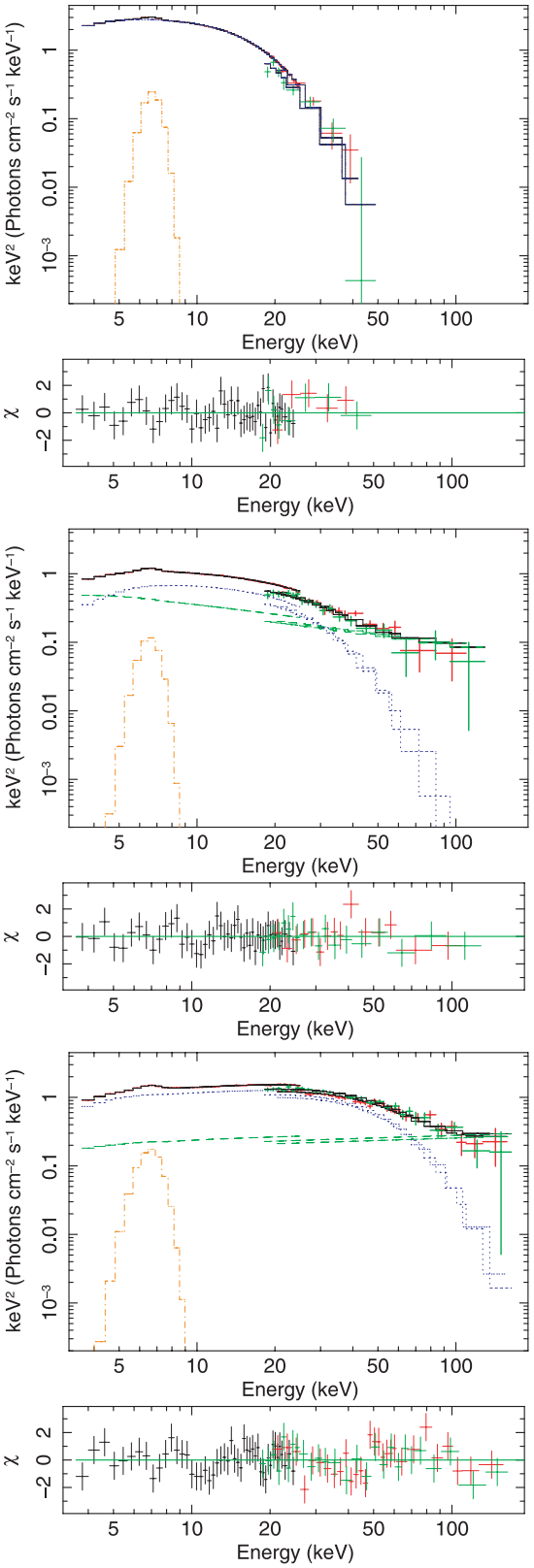

Figure 5. *INTEGRAL*/IBIS (green data) and *RXTE*/PCA and HEXTE (red data) spectra of 4U 1728–34: spe6, spe3 and spe1 data sets from top to bottom, with data, models and residuals to the models with the χ value. The model is Gaussian plus Comptonization for spe6, and Gaussian, Comptonization plus power-law component for spe3 and spe1.

Table 2. Other spectral fitting results for the hard state spectra of 4U 1728–34 with simultaneous *INTEGRAL* and *RXTE* observations.

	spe1	spe2	spe3
Parameters	CompPS+diskbb (5)		
$kT_{\rm in}$ (keV)	$1.11^{+0.04}_{-0.14}$	$1.04^{+0.04}_{-0.05}$	$0.93^{+0.02}_{-0.02}$
$\rm norm_{diskbb} \times 10^{-2}$	39 (fx)[a]	47 (fx)	107 (fx)
$kT_{\rm e}$ (keV)	$26.84^{+0.78}_{-0.22}$	$24.20^{+1.15}_{-1.44}$	20 ± 3.7
$kT_{\rm bb}$ (keV)	$1.47^{+0.08}_{-0.17}$	$1.46^{+0.08}_{-0.09}$	$1.53^{+0.05}_{-0.04}$
τ_y	3.0 ± 1.24	2.83 ± 0.31	$2.43^{+0.06}_{-0.18}$
$\Omega/2\pi$	1.0 ± 0.43	1 ± 0.37	1 ± 0.57
$\rm norm_{CompPS}$	$55.36^{+38.82}_{-11.53}$	$42.32^{+13.36}_{-8.80}$	$35.83^{+4.60}_{-4.20}$
$\chi^2_r(\nu)$	0.77(95)	0.78(84)	0.69(75)
Parameters	CompTT+diskbb+reflect (6)		
$\Omega/2\pi$	$1.27^{+0.38}_{-0.27}$	$1.20^{+0.40}_{-0.22}$	$1.51^{+0.40}_{-0.36}$
kT_0 (keV)	$1.14^{+0.04}_{-0.05}$	$1.19^{+0.02}_{-0.03}$	$1.45^{+0.41}_{-0.04}$
$kT_{\rm e}$ (keV)	$30.66^{+26.03}_{-8.24}$	28.82 ± 13.50	28.47 ± 14.90
τ	$0.76^{+0.42}_{-0.46}$	$0.70^{+0.38}_{-0.02}$	0.39 ± 0.33
$\rm norm_{CompTT} \times 10^{-2}$	$1.63^{+0.74}_{-0.82}$	$1.27^{+0.18}_{-0.02}$	$0.97^{+0.85}_{-0.68}$
$kT_{\rm in}$ (keV)	$0.73^{+0.03}_{-0.04}$	$0.77^{+0.01}_{-0.03}$	$0.95^{+0.01}_{-0.01}$
$\rm norm_{diskbb} \times 10^{-2}$	236 (fx)	191 (fx)	115 (fx)
$\chi^2_r(\nu)$	0.74(95)	0.78(84)	0.71(75)

[a](fx) are fixed parameters.

described in the following models (4a) and (4b). In both cases, to fit the data using the double blackbody it is necessary to freeze the soft component parameters (either the temperature or the normalization values) otherwise the fits with the double blackbody model are not constrained. Moreover, the double blackbody is not any more necessary for the hard states (in fact just one bb is sufficient to take into account the soft emission).

(4a) bb+diskbb+bknpower+highecut models

We try a phenomenological model (used in Lin et al. 2007 and motivated by similarities with the BH systems) composed by two thermal components, a blackbody and a multicolour disc blackbody, plus a broken power law (bknpower) with high-energy cut-off (highecut).

Results for all the spectra are reported in Table 1. Freezing the soft parameters (blackbody normalizations), we obtain fits with a monotonic spectral evolution of the parameters from the soft to the hard states. The blackbody temperature, $kT_{\rm bb}$, decreases monotonically from the soft to the hard states, while the second soft disc blackbody component is detected only in the softer states.

(4b) bb+diskbb+CompTT+PL models

The hard components to be added to the double blackbody components could be described as a Comptonization model plus an additional power law that is required for the hard states only. The results are reported in Table 1. Also in this case we have the same evolution of the soft parameters (blackbody temperatures) but, in addition, we get the physical information about the origin of the hard component. The electron temperature of the corona increases and the optical depth decreases as the spectrum becomes harder, while the temperature of the seed input photons remains constant.

Even if there is a monotonic physical evolution of the soft parameters (blackbody temperature increases from hard to soft states), models (4a) and (4b) are not well constrained; in fact, to obtain a good fit we need to freeze the normalization value of the blackbody.

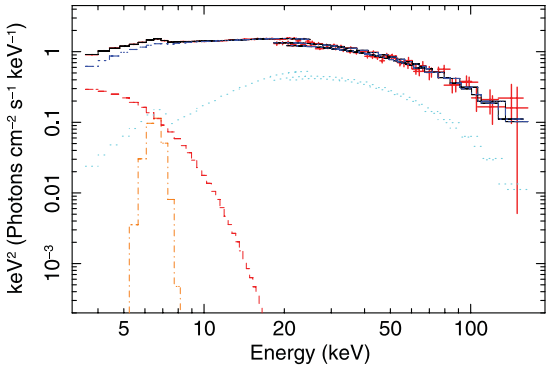

Figure 6. Spectrum of the spe1 data set with Gaussian, diskbb plus CompPS model assuming a hybrid thermal and non-thermal electron distribution.

2.3.1 *Further models for the hard states*

The presence of high-energy residual to the Comptonization model for the hard states, spe1–spe3, prompted us to try other models also.

(5) diskbb+CompPS models

The CompPS model (Poutanen & Svensson 1996), which takes into account the Comptonized processes with non-thermal distribution of the velocities of the electrons, was used to model some binary systems showing non-thermal component. So we combine a disc blackbody component and a CompPS modelled with the assumption of a hybrid thermal and non-thermal composition of the electron plasma in a corona, which takes into account the high-energy excess, and a good fit has been obtained. The result is a Comptonizing plasma, assumed to be of spherical geometry, with $kT_{\rm e} \simeq 20$–27 keV, optical depth $\tau_y \simeq 2.4$–3, input seed photons with $kT_{\rm bb} \simeq 1.5$ keV, reflection factor, $\Omega/2\pi$, of 1, inner disc temperature of 1 keV and the high-energy tail with electron power-law index $p \simeq 0.6$, 1.37 and 3.2, respectively, for spe3, spe2 and spe1 above the electron Lorentz factor of 1.6. Results are reported in Table 2. We show the energy spectra with these models for the hardest spectrum (spe1) in Fig. 6.

The unabsorbed bolometric fluxes of the spe1 and spe3 spectra are 8.5×10^{-9} and 5.8×10^{-9} erg cm^{-2} s^{-1} corresponding to bolometric luminosities of 2.1×10^{37} and 1.5×10^{37} erg s^{-1}.

(6) diskbb+CompTT+reflect models

An alternative model for the hard states consists in adding a reflection component, reflect (Magdziarz & Zdziarski 1995), to Comptonization and blackbody. In this case, the Comptonization component requires input seed photons with a temperature of 1.1–1.5 keV, a corona with a higher electron temperature, ranging from 28 to 31 keV, and a lower optical depth of 0.4–0.8 with respect to model (3). The inner disc blackbody temperature is 0.7–0.9 keV and the reflection component, which fits the bump near 20–30 keV, has a high reflection factor of 1.2–1.5. We show the energy spectra of the hardest spectrum (spe1) with these alternative models in Fig. 7. This model gives acceptable $\chi^2_r(\nu)$ as reported in Table 2.

This model gives a high reflection fraction which would imply a small inner disc radius not usually observed in the hard state and that makes this model difficult to consider (for a discussion of inner radii of accretion disc in hard state, see e.g. Reis et al. 2010 and also Done & Gierlinski 2006). Moreover, no indication of such strong reflection feature was observed by *Chandra* (even if below 10 keV) for this source and in general this high value has not been detected so far in the atoll class.

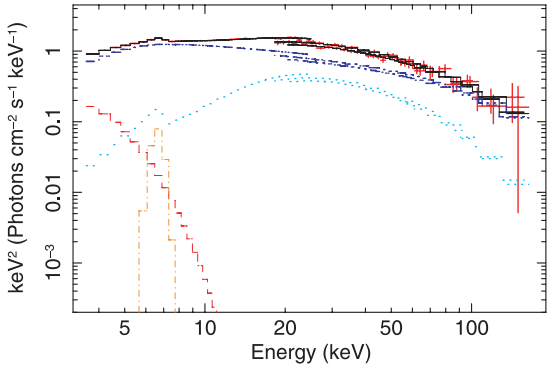

Figure 7. Spectrum of the spe1 data set with Gaussian, diskbb, Comptonization plus high reflection component.

3 DISCUSSION AND CONCLUSIONS

The simultaneous *RXTE* and *INTEGRAL* long monitoring observations allow us to study over a broad energy band (3–200 keV) the different spectral states of 4U 1728–34 selected according to the position on the PCA HID, as well by the *INTEGRAL* high-energy behaviour of the source.

In general, the observed spectra of 4U 1728–34 turned out to be difficult to model. In particular, at low energy the presence of the blackbody or disc blackbody emission is difficult to constrain because the PCA is sensitive for $E > 4$ keV, and at high energy there seems to be a non-thermal component during the hard state that needs to be investigated.

A number of models provide statistically satisfactory fits to our data. We prefer models that provide spectral parameters with physical meaning and at the same time evolve regularly through the source states.

The simplest spectral model that describes well the observed spectral states is the sum of blackbody and Comptonization (CompTT) emission for the soft states and Comptonization with the addition of the power law for the hard states.

In the soft spectra, the Comptonization would arise from a corona with a low electron temperature of about 4–7 keV and high optical depth of 2–3, with input seed photons of temperature 0.6–0.8 keV. The blackbody temperature $kT_{\rm bb}$ is 2.3–2.5 keV and consistently higher than the seed photons temperature which gives rise to the Comptonization processes. This indicates that the blackbody emission could come either from inner parts of the disc or from the boundary layer, while the seed photons could be due to the emission from the outer part of the disc or from the NS surface directly. The compatibility of the boundary layer temperature predicted from the spreading layer model (Suleimanov & Poutanen 2006) with the obtained $kT_{\rm bb}$ supports the hypothesis that the blackbody component originates from the boundary layers.

Only the most luminous soft state could also be modelled with a double thermal emission (simple blackbody plus disc blackbody emission). In this last case the temperature of the blackbody is still compatible with the boundary layer emission, while the disc emission has lower temperature (1.7 keV) and would come from the outer part of the disc.

The hard spectra can be described by a thermal Comptonization with a temperature of the electrons of ∼6–10 keV and optical depth of 3, plus a power law with photon index of ∼1.8–2.5. As the spectrum becomes harder, the temperature of the electrons increases and the optical depth decreases. The seed photon temperature does not change much during the soft to hard spectral variation indicating the same emission region (in this case the hypothesis of the NS emission origin could be suitable).

By combining the results of these two models for the hard and soft states, we note that the variation of the physical parameters values is quite monotonic (within the error values). During the hardening the blackbody temperature, $kT_{\rm bb}$, decreased (until it is no longer detected in the hardest states), the Comptonization component increased in temperature, $kT_{\rm e}$, and decreased in optical depth, τ, while the seed photons temperature value, kT_0, did not vary significantly.

The detection of a hard tail component for this atoll source, even if not the emission prominent in our data, represents an important result, but our data do not allow us to establish a proper origin. The detection of radio emission during the hard state could indicate the link of this non-thermal emission with a jet formation (Migliari et al. 2007). In fact, as the BHBs show hard states associated with jet formation, this could be also the case for atoll sources. Radio emission was already observed from 4U 1728–34 but unfortunately during our observations no radio coverage was available for this source.

Alternatively, the hard states could be also modelled by a blackbody component with temperature of 1 keV plus a Comptonization (CompPS) with higher electron temperature (20–26 keV) and a high-energy tail due to a hybrid thermal–non-thermal composition of the electron plasma. Hence, the hybrid thermal–non-thermal composition of the electron population in the corona appears as a plausible explanation for the hard tails detected.

We found that the hard states could also be modelled without the use of the Comptonization component but with the use of the phenomenological model consisting of a blackbody plus a broken power law with a high-energy cut-off as already used by Lin et al. (2007).

In the hardest spectrum (spe1), the relative flux contribution above $E > 60$ keV is about 10 per cent, i.e. similar to the value in the hard state of 4U 1820–30 and, in general, is of the same order of other hard tail flux contribution in NS systems (Migliari et al. 2007; Tarana et al. 2007).

Finally, we note that this source presents flux variations that do not always reach the same value of hardness, as shown by the HID. This indicates that the hardest spectrum characterized by the power-law component cannot always be reached by the source; this could explain the difficulty in detecting this component in previous observations of the source. This could be due to an additional parameter, hitherto unknown, driving spectral variation besides the accretion rate (Homan et al. 2001).

ACKNOWLEDGMENTS

This research has made use of data obtained with *INTEGRAL* which is an ESA project with instruments and science data centre funded by ESA member states especially the PI countries: Denmark, France, Germany, Italy, Switzerland, Spain, Czech Republic and Poland, and with the participation of Russia and the USA. The authors thank M. Federici for the continuous effort to update the *INTEGRAL* archive and software in Rome, and L. Natalucci for the scientific and data analysis support. A special thanks to J. Homan who gives important scientific contribution to the paper and in particular to the spectral fitting procedure. The authors also thank A. Paizis for the information and discussion about the applicability of the compTB model to the hard spectral state. The research leading to these results has received funding from the European Community's Seventh Framework Programme (FP7/2007-2013) under grant agreement

number ITN 215212 Black Hole Universe. We acknowledge the ASI financial support via grant ASI-INAF I/008/07.

REFERENCES

Arnauld K. A., 1996, in Jacoby G. H., Barnes J., eds, ASP Conf. Ser. Vol. 101, Astronomical Data Analysis Software and Systems V. Astron. Soc. Pac., San Francisco, p. 17
Claret A. et al., 1994, ApJ, 423, 436
Courvoisier T. J.-L. et al., 2003, A&A, 411, L53
D'Aí A., Iaria R., Di Salvo T., Lavagetto G., Robba N. R., Burderi L., Mendez M., van der Klis M., 2005, in Burderi L., Antonelli L. A., D'Antona F., Di Salvo T., Israel G. L., Piersanti L., Tornambè A., Straniero O., eds, AIP Conf. Proc. Vol. 797, Interacting Binaries: Accretion, Evolution and Outcomes. Am. Inst. Phys., New York, p. 545
D'Aí A. et al., 2006, A&A, 448, 817
Di Salvo T., Stella L., 2002, in Goldwurm A., Neumann D., Trân Thanh Vân J., eds, Proc. Moriond Astrophys. Meeting, The Gamma-Ray Universe. Gioi Pub., Vietnam, preprint (astro-ph/0207219v1)
Di Salvo T. et al., 2000a, ApJ, 544, L119
Di Salvo T., Iaria R., Burderi L., Robba N. R., 2000b, ApJ, 542, 1034
Di Salvo T., Robba N. R., Iaria R., Stella L., Burderi L., Israel G. L., 2001a, ApJ, 554, 49
Di Salvo T., Mendez M., van dre Klis M., Ford E., Robba N. R., 2001b, ApJ, 546, 1107
Done C., Gierlinski M., 2006, MNRAS, 367, 659
Falanga M., Götz D., Goldoni P., Farinelli R., Goldwurm A., Mereghetti S., Bazzano A., Stella L., 2006, A&A, 458, 21
Farinelli R., Frontera F., Virgilli E., Falanga M., Goldoni P., Goldwurm A., 2004, in ESA SP-552. ESA, Noordwijk, p. 317
Farinelli R., Titarchuk L., Frontera F., 2007, ApJ, 662, 1167
Farinelli R., Titarchuk L., Paizis A., Frontera F., 2008, ApJ, 680, 602
Fender R. P., 2006, in Lewin W. H. G., van der Klis M., eds, Compact Stellar X-ray Sources. Cambridge Univ. Press, Cambridge
Fiocchi M., Bazzano A., Ubertini P., Jean P., 2006, ApJ, 651, 416
Forman W., Tananbaum H., Jones C., 1976, ApJ, 206, L29
Galloway D. K., Psaltis D., Chakrabarty D., Muno M. P., 2003, ApJ, 590, 999
Goldwurm A. et al., 2003, A&A, 411, L223
Grindlay J. E., Hertz P., 1981, ApJ, 247, L17
Hasinger G., van der Klis M., 1989, A&A, 225, 79
Hoffman J. A., Lewin W. H. G., Doty J., Hearn D. R., Clark G. W., Jernigan G., Li F. K., 1976, ApJ, 210, L13
Homan J., Belloni T., 2005, Ap&SS, 300, 107
Homan J., Wijnands R., van der Klis M., Belloni T., van Paradijs J., Klein-Wolt M., Fender R., Méndez M., 2001, ApJS, 132, 377
Iaria R., Di Salvo T., Burderi L., Robba N. R., 2001, ApJ, 548, 883
Lewin W. H. G., Clark G. W., Doty J., 1976, IAU Circ., 2922, 1
Lin D., Remmilard R. A., Homan J., 2007, ApJ, 667, 1073
Magdziarz P., Zdziarski A. A., 1995, MNRAS, 273, 837
Markoff S., Nowak M. A., Wilms J., 2005, ApJ, 635, 1203
Martí J., Mirabel I. F., Rodriguez J., Chaty S., 1998, A&A, 332, L45
Migliari S., Fender R. P., 2006, MNRAS, 366, 79
Migliari S., Fender R. P., Rupen M., Jonker P. G., Klein-Wolt M., Hjellming R. M., van der Klis M., 2003, MNRAS, 342, L67
Migliari S. et al., 2007, ApJ, 671, 706
Mitsuda K. et al., 1984, PASJ, 36, 741
Mitsuda K., Inoue H., Nakamura N., Tanaka Y., 1989, PASJ, 41, 97
Piraino S. A., Santangelo A., Kaaret P., 2000, A&A, 360, L35
Piraino S. A., 1999, A&A, 349, 77
Poutanen J., Coppi P., 1998, Phys. Scr., T77, 57
Poutanen J., Svensson R., 1996, ApJ, 470, 249
Reis R. C., Fabian A. C., Miller J. M., 2010, MNRAS, 402, 836
Suleimanov V., Poutanen J., 2006, MNRAS, 369, 2036
Tarana A., Bazzano A., Ubertini P., Zdziarski A. A., 2007, ApJ, 654, 494
Titarchuk L., 1994, ApJ, 434, 570
Titarchuk L., Zannias T., 1998, ApJ, 493, 863
van Straaten S., van der Klis M., Di Salvo T., Belloni T., 2002, ApJ, 568, 912
White N. E., Peacock A., Hasinger G., Mason K. O., Manzo G., Taylor B. G., Brandurdi-Raymont G., 1986, MNRAS, 218, 129

This paper has been typeset from a TEX/LATEX file prepared by the author.